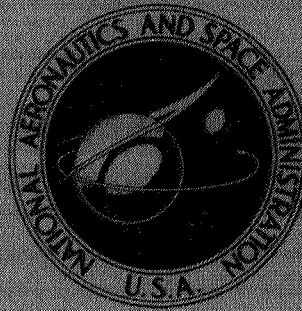


**NASA TECHNICAL  
MEMORANDUM**



**NASA TM X-2990**

**NASA TM X-2990**

**STEADY-STATE INLET TEMPERATURE  
DISTORTION EFFECTS ON THE STALL LIMITS  
OF A J85-GE-13 TURBOJET ENGINE**

*by Charles M. Mehalic and Roy A. Lottig*

*Lewis Research Center  
Cleveland, Ohio 44135*

1. Report No. <b>NASA TM X-2990</b>		2. Government Accession No.		3. Recipient's Catalog No.	
4. Title and Subtitle <b>STEADY-STATE INLET TEMPERATURE DISTORTION EFFECTS ON THE STALL LIMITS OF A J85-GE-13 TURBOJET ENGINE</b>				5. Report Date <b>February 1974</b>	
				6. Performing Organization Code	
7. Author(s) <b>Charles M. Mehalic and Roy A. Lottig</b>				8. Performing Organization Report No. <b>E-7626</b>	
9. Performing Organization Name and Address <b>Lewis Research Center National Aeronautics and Space Administration Cleveland, Ohio 44135</b>				10. Work Unit No. <b>501-24</b>	
				11. Contract or Grant No.	
12. Sponsoring Agency Name and Address <b>National Aeronautics and Space Administration Washington, D. C. 20546</b>				13. Type of Report and Period Covered <b>Technical Memorandum</b>	
				14. Sponsoring Agency Code	
15. Supplementary Notes					
16. Abstract <p>The effects of circumferential and radial temperature distortions and combined temperature and pressure distortion on the performance of a J85-GE-13 turbojet engine were investigated. In terms of loss of compressor pressure ratio at stall, the most severe pattern of temperature distortion was hub radial while a circumferential pattern of diametrically opposed sectors was least severe. The effect of combined temperature and pressure distortion was dependent on the location of the high temperature and low pressure regions. The most serious stall pressure ratio losses occurred when these regions coincided.</p>					
17. Key Words (Suggested by Author(s)) <b>Turbojet engine; Temperature distortion; Combined pressure and temperature distortion; Compressor stall pressure ratio loss; Steady-state stall limits</b>			18. Distribution Statement <b>Unclassified - unlimited</b>		
19. Security Classif. (of this report) <b>Unclassified</b>		20. Security Classif. (of this page) <b>Unclassified</b>		21. No. of Pages <b>38</b>	22. Price* <b>\$3.00</b>

\* For sale by the National Technical Information Service, Springfield, Virginia 22151

# STEADY-STATE INLET TEMPERATURE DISTORTION EFFECTS ON THE STALL LIMITS OF A J85-GE-13 TURBOJET ENGINE

by Charles M. Mehalic and Roy A. Lottig

Lewis Research Center

## SUMMARY

An experimental investigation was made to determine the effects of temperature distortions, alone and in combination with total pressure distortion, on a J85-GE-13 turbojet engine. A gaseous hydrogen fueled burner produced the circumferential and radial temperature distortions. Combined distortions were induced with a screen coupled with the burner. The loss of compressor stall pressure ratio at constant speed was used to determine the severity of the various distortions tested. Hub radial temperature distortions caused the largest loss of stall pressure ratio and a pattern of diametrically opposed  $90^\circ$  sectors caused the smallest losses. The effect of combined temperature and pressure distortion was dependent on the relative locations of the high temperature and low pressure regions. The most severe effect occurred when the high temperature and low pressure regions coincided (to provide the lowest air density) and the least effect was realized when these regions were diametrically opposed (thus reducing variations in air density).

## INTRODUCTION

One of the problems that must be considered in the development of advanced aircraft engines is the detrimental effect on compressor operating limits and performance caused by inlet temperature distortions. This problem is of particular concern in applications where ingestion of hot gases from armament firing, flight maneuvers, or recirculation from VTOL-type aircraft may be encountered. Also, higher pressure ratio fans on new engines, while attenuating inlet pressure distortions, may create significant temperature distortions at the core compressor inlet.

Extensive effort has been exerted to evaluate the effects of inlet pressure distortions on the performance of engine compressor systems. (Refs. 1 to 3 represent a

typical sampling of this effort.) Much less effort has been focused on defining and analyzing the effect of nonuniform inlet temperature distributions on compressor performance. Some examples of temperature distortion effects on aircraft engines are contained in references 4 and 5.

This investigation is part of a program at the Lewis Research Center to study the effects of nonuniform inlet flow conditions on engine stability limits. This report is concerned with the effect of steady-state spatial inlet temperature distortions on the stability limits of a J85-GE-13 turbojet engine. A gaseous hydrogen fueled burner was used upstream of the engine to produce the temperature distortions.

The investigation was conducted with circumferential temperature distortions of  $90^\circ$ ,  $180^\circ$ , and  $270^\circ$  extent and a pattern of diametrically opposed  $90^\circ$  sectors. The effect of a  $360^\circ$  extent hub radial distortion was also investigated. In addition, data were obtained for a  $180^\circ$  extent circumferential temperature distortion combined with a  $180^\circ$  extent circumferential pressure distortion produced by a screen. All tests were performed in an altitude facility at an engine inlet Reynolds number index of 0.65; the  $180^\circ$  extent circumferential pattern was also tested at an index of 0.30.

## APPARATUS AND INSTRUMENTATION

### Facility

The test program was conducted in an altitude chamber of the Propulsion Systems Laboratory at the Lewis Research Center. This facility has the capability of simulating altitudes from sea level to 24 390 meters (80 000 ft) with airflow rates of 218 and 22.7 kilograms per second (480 and 50 lb/sec), respectively.

A photograph of the test installation is shown in figure 1. The engine was mounted on a thrust stand in the chamber with the inlet duct passing through a labyrinth seal in the forward bulkhead. A direct-connect installation was utilized with the inlet air bellmouth mounted in the plenum upstream of the forward bulkhead. The bellmouth was designed to have a throat Mach number of 0.6 at rated engine airflow.

### Engine

The General Electric J85-GE-13 used in this investigation is an afterburning turbojet engine with a thrust to weight ratio of 7.2 with maximum afterburning at sea level. The engine consists of an eight-stage axial flow compressor coupled to a two-stage turbine,

an annular combustor, an afterburner (not used in this test), and a variable area exhaust nozzle.

The compressor has variable inlet guide vanes which are mechanically linked to the interstage (3rd, 4th, and 5th) bleed valves so that the vanes are deflected the greatest when the valves are fully open. The inlet guide vane-interstage bleed schedule is a function of the inlet temperature and corrected engine speed. The average inlet temperature, sensed by eight thermocouples connected in parallel around the engine face, was used as the input to control the inlet guide vanes and interstage bleeds for this test. Normally the bleed valves are scheduled from full open at 80 percent corrected speed to full closed at 94 percent corrected speed. For this investigation the schedule was modified to provide the bleed variation between 76 and 90 percent corrected speed. The normal and modified bleed schedules are shown in figure 2. This modified bleed schedule is the maximum allowable bleed closure for safe engine operation and was required to obtain many of the stalls at low corrected speeds.

To avoid overtemperaturing the turbine while inducing compressor stalls, the first-stage turbine nozzle was replaced with one that was approximately 26 percent smaller in area than the standard nozzle. This rematched the turbine to the compressor at a lower turbine inlet temperature for any operating point on the compressor map.

The exhaust nozzle area was manually controlled during the test program. Six area blockage plates (fig. 1) were installed on the nozzle leaves to obtain areas less than permitted by the standard nozzle. These smaller areas were required to obtain compressor stall at the low speeds with low levels of distortion.

### Temperature Distortion Generator

A gaseous hydrogen fueled burner was used to produce the compressor inlet temperature distortion patterns. Hydrogen was used because of its good ignition characteristics and rapid flame propagation speed. The burner was installed in the plenum upstream of the inlet air bellmouth. A schematic of the hydrogen supply system and a photograph of the burner are shown in figure 3. Engine inlet airflow was heated as it passed through the burner which was divided into four 90° sectors. Each sector contained five annular V-gutters (fig. 3). Hydrogen was supplied through a tubing system located in the gutters and fed by a separate supply manifold for each sector. The flow of hydrogen to each gutter in a sector was controlled by valves located downstream of the manifold. Each sector contained five swirl-can pilot burners to provide an ignition source for the main hydrogen flow. A slow response, remote operated control valve was used to vary hydrogen flow and provide temperature control. Each sector had its own control system which permitted operation of from one to four sectors so that

patterns from  $90^{\circ}$  to  $360^{\circ}$  of circumferential extent could be generated. Also, by shutting off hydrogen flow to the gutters near the outer wall, hub radial temperature distortion patterns were produced.

### Instrumentation

The instrumentation type, number, and location in the installation are shown in figure 4 together with a schematic of the engine. The temperature measurements at the compressor inlet were 4.45 centimeters (1.75 in.) upstream of the engine inlet. The inlet static and total pressures and the inlet guide vane and interstage bleed control temperatures were not in the same plane as the inlet temperature measurements to minimize the blockage at the inlet. The inlet static pressures, total pressures, and guide-vane control temperatures were 6.99, 9.21, and 20.96 centimeters (2.75, 3.63, and 8.25 in.), respectively, upstream of the engine inlet. In this report these four axial instrumentation locations at the compressor inlet will be referred to as station 2. The 60 thermocouples (12 rakes  $\times$  5 elements/rake) at the compressor inlet and those at station 3 were bare wire, Chromel-Alumel thermocouples designed in accordance with the guidelines established in reference 6 and fabricated from 0.0076 centimeter (0.003-in.) diameter wire.

Pressures, temperatures, and engine operating parameters were recorded on the Lewis Central Automatic Digital Data Encoder (CADDE). Details of this recording system are given in reference 7.

### PROCEDURE

The engine was initially run with no inlet distortion to establish baseline data. For these tests, conditioned air was supplied to the inlet duct at a total pressure and temperature of  $68\,948\text{ N/m}^2$  (10 psia) and  $297.2\text{ K}$  ( $535^{\circ}\text{ R}$ ) to obtain an engine-inlet Reynolds number index (ReI) of approximately 0.65. Base data were also recorded at a ReI of 0.30. In all cases the altitude chamber pressure was maintained just low enough to ensure exhaust nozzle operation at critical flow. Stall data were obtained by reducing the exhaust nozzle area while maintaining constant corrected engine speed.

To obtain compressor maps and stall data with temperature distortion, the engine was operated at the minimum obtainable compressor pressure ratio at the desired rotor speed and the magnitude and extent of the inlet temperature distortion was established by regulating hydrogen flow to the burner. The compressor was then forced to operate at increasingly higher pressure ratios by making incremental reductions of exhaust

nozzle area while corrected speed was held constant. Steady-state data were recorded at each nozzle area and turbine discharge temperature was monitored at each data point and at the stall point.

Compressor stall data were obtained for circumferential temperature distortions of  $90^\circ$ ,  $180^\circ$ , and  $270^\circ$  extent and a hub radial pattern that distorted approximately 50 percent of the annular passage at the compressor inlet. Investigations were carried out over a range of corrected speeds from 85 to 100 percent of rated with distortion amplitudes up to 21 percent of the average absolute inlet temperature. All tests were conducted at an average inlet Reynolds number index of 0.65 with the exception of the  $180^\circ$  extent circumferential pattern which was also tested at a ReI of 0.30. The symbols used in this report are defined in appendix A and the methods of calculation are described in appendix B.

## RESULTS AND DISCUSSION

The results presented are for a J85-GE-13 turbojet engine that was modified as discussed earlier (see the section APPARATUS AND INSTRUMENTATION). The smaller turbine nozzle area does not effect the compressor stall line but moves the operating line closer to stall for a given exhaust nozzle area. The modified inlet guide vane - interstage bleed schedule could have some effect on the stall line at corrected speeds below 94 percent. The results are presented in terms of compressor stall pressure ratio loss and do not depend on the compressor operating line. Therefore, for corrected speeds greater than or equal to 94 percent, the results are applicable to a standard engine. The results presented for corrected engine speeds less than 94 percent could differ from those that would be obtained with a standard engine but can be compared with the results of pressure distortion tests (ref. 1) which were obtained with the same engine modifications.

### Inlet Profiles

The temperature patterns generated at the engine inlet with the hydrogen burner heating all the air passing through it are shown in figure 5. The radial and circumferential profiles are presented for airflow rates corresponding to 100 and 90 percent of the rated mechanical speed of the engine. The radial variation represents the average of all measurements at the same immersion depth ratioed to the average temperature at station 2. Likewise, the circumferential variation is the average of all measurements on a rake ratioed to station 2 average temperature. Data are presented for three levels

of temperature rise across the burner at each engine speed and in all cases the maximum variation, either radially or circumferentially, is approximately 2 percent. These profiles represent the final adjustment of the valves downstream of the hydrogen supply manifolds (fig. 3) in attempting to obtain a uniform temperature rise across the burner.

A circumferential temperature distortion pattern of  $180^\circ$  extent, produced by heating the inlet airflow passing through two adjacent sectors of the burner, is shown in figure 6. All the temperature measurements at the compressor inlet are presented as ratios to the average temperature. The variations of temperature in the profile are typical of all the circumferential distortion patterns that were generated. Also superimposed on figure 6 are the station 2 total pressures ratioed to their average value. The pressures indicate that no inlet pressure distortion was present which was observed to be true with all temperature distortion patterns investigated.

Examples of the circumferential temperature distortions that were imposed at the compressor inlet for this program are presented in figure 7. Radial and circumferential gradients as defined for figure 5 are shown for  $90^\circ$ ,  $180^\circ$ , and  $270^\circ$  extents and a two-per-revolution pattern of  $90^\circ$  extents. The radial gradients (1 to 2 percent) existed with all circumferential patterns.

A typical pattern of hub radial temperature distortion is shown in figure 8. Both the individual measurements (fig. 8(a)) and the average gradients (fig. 8(b) and 8(c)) are presented.

### Compressor Maps with Uniform Inlet Flow

Compressor performance maps for ReI's of 0.65 and 0.30 with uniform inlet flow conditions are presented in figure 9. The lines of constant exhaust nozzle area were obtained from cross-plotted data of pressure ratio and corrected flow as a function of  $A_8$  for each engine speed. The discontinuity in the constant area lines at 90 percent corrected speed was caused by the modified inlet guide vane - interstage bleed schedule used in this investigation. At this speed the interstage bleed just became full-closed while the guide vanes became full open when increasing speed.

The effect of reducing the engine-inlet Reynolds number index is apparent by comparing the compressor maps of figures 9(a) and 9(b). The stall line for the reduced ReI is shifted downward on the map and a given operating point (that is, corrected speed and exhaust nozzle area) is moved to a lower airflow at about the same pressure ratio. Consequently, the reduced Reynolds number index causes the compressor to operate closer to its stall limit.

For ease of reference, the undistorted stall line and 0.0839-square-meter (130-in.<sup>2</sup>) exhaust nozzle area line are reproduced on subsequent compressor maps. Also included

are lines of constant corrected speed, from cross plots, which correspond to the same speeds as the data.

### Circumferential Distortion Patterns

The effect of  $90^\circ$  extent circumferential temperature distortions on compressor performance at an inlet Reynolds number index of 0.65 is shown in figure 10. Corrected values of engine speed and inlet airflow were calculated using the average pressure and temperature at the engine inlet. Distortion amplitude was calculated by ratioing the difference of the local maximum and minimum temperatures to the average inlet temperature. The lowest distortion amplitudes, approximately 6 percent, produced small degradations in compressor stall pressure ratio. The major effect of the low distortion amplitudes was to cause a loss in the airflow pumping capability of the compressor. Increasing the distortion amplitude caused larger effects on both stall pressure ratio and pumping capability. The highest distortion levels investigated (approximately 20 percent, fig. 10(c)) show a severe effect on compressor performance. The decrease in pumping capability is accompanied by a large decrease in pressure ratio at stall.

The results of the tests with  $180^\circ$  extent circumferential distortions at an inlet ReI of 0.65 are presented in figure 11. Three distortion amplitudes were investigated and the stall line and pumping capability trends are very similar to those discussed for the  $90^\circ$  extent distortions. The average inlet temperature used in the calculation of corrected speed limited the corrected speed range when large distortion amplitudes were imposed at the compressor inlet. This is evident in figure 11(c) where a maximum corrected speed of 96.2 percent was obtained with the engine operating at rated mechanical speed.

The effect of  $270^\circ$  extent circumferential inlet temperature distortion on compressor performance at a ReI of 0.65 is shown in figure 12. The trends appear to be the same as those discussed for the previous circumferential patterns but the effect is not quite as severe. The stall at 88.3 percent corrected speed with the largest distortion amplitude (fig. 12(c)) occurred immediately after the data were recorded and before the engine settings could be changed. All the other stall points were obtained by the extrapolation procedure discussed in appendix B.

A pattern of two diametrically opposed  $90^\circ$  sectors was investigated at an inlet Reynolds number index of 0.65 and the compressor maps of figure 13 were obtained. Data were recorded for several distortion levels at rated mechanical speed and at approximately 87 percent corrected speed. This pattern exhibits trends similar to those of figure 10 (single  $90^\circ$  sector) but the multiple pattern is not as detrimental to performance as the one-per-revolution pattern, especially at the high distortion levels.

Here again the maximum attainable corrected speed was limited to 95 percent because of the elevated average temperature with the large distortion amplitude.

As stated earlier, the  $180^\circ$  extent pattern was also investigated at an average inlet Reynolds number index of 0.30. Compressor maps showing the performance at this index are presented in figure 14. The net effect, as discussed earlier, of operating at a reduced ReI without distortion is to make the compressor operate closer to stall for a given exhaust nozzle area. A comparison of figure 14(b) with 11(b) shows that with approximately the same distortion level there is a greater reduction of stall pressure ratio at the low ReI while the reduction in pumping capability is about the same for either index. Therefore, the effect of inlet temperature distortion is more severe when operating at reduced values of ReI.

### Radial Distortion Patterns

Although the temperature distortion generator was originally designed to produce circumferential distortions, in the process of testing it was also found that hub radial distortions could be generated. Data obtained with this type of distortion at an inlet ReI of 0.65 are presented in figure 15. With low distortion levels of about 7 to 8 percent there is little effect on either the stall pressure ratio or airflow pumping capability of the compressor. In fact, results show the only effect at the middle of the speed range is a small reduction in the airflow capability of the compressor. With higher distortion levels of about 14 percent (fig. 15(b)) the results are similar to those of the circumferential patterns. Both the stall pressure ratio and pumping capability show significant reductions even with the moderate levels of distortion investigated.

### Compressor Stall Pressure Ratio Loss

The loss of compressor stall pressure ratio as a function of the distortion amplitude is presented in figure 16 for the patterns tested at a Reynolds number index of 0.65. The stall pressure ratio loss,  $\Delta PRS$ , used in this correlation is defined as the difference between the undistorted and distorted pressure ratios at stall divided by the undistorted stall pressure ratio. The pressure ratios at stall, from the compressor maps, are at the same corrected speed for the distorted and undistorted stall points. Therefore, changes in airflow caused by the distortion affect the value of  $\Delta PRS$ . The descriptor of distortion level was calculated by ratioing the difference of the local maximum and minimum temperatures to the average inlet temperature.

All of the distortion patterns of figure 16 except the two-per-revolution show that

$\Delta$ PRS is a function of corrected speed. For these cases the value of  $\Delta$ PRS is higher at corrected speeds below 90 percent. The reason for  $\Delta$ PRS being a function of speed for these distortion patterns can probably be explained by the fact that the interstage bleed and inlet guide vane settings are variable below 90 percent speed and  $\Delta$ PRS is based on an undistorted stall line obtained with the schedule of figure 2. Since the schedule is controlled by average temperature, the distorted portion of the compressor, which dictates where stall occurs, is operating off schedule closer to stall because of its elevated inlet temperature and lower corrected speed. Because of this off-schedule operation combined with the distortion, the compressor average stall point occurs at a lower distortion level than expected. This has the result then of giving high values of  $\Delta$ PRS when operating with temperature distortion in the speed range where the guide vanes and interstage bleeds are functioning because the method of calculating  $\Delta$ PRS does not account for off-schedule operation.

A summary of the effect of the various distortions on  $\Delta$ PRS is presented in figure 17 for speeds greater than 90 percent. The largest loss of compressor stall pressure ratio was caused by the hub radial distortion with a  $\Delta$ PRS of approximately 0.08 for a 15 percent distortion amplitude. The multiple pattern and the 270° extent circumferential distortion, which both resulted in a  $\Delta$ PRS of approximately 0.04 for a 15 percent temperature distortion, have the smallest effect on compressor performance.

#### Inlet Temperature Sensor Location

The data presented so far were obtained with the interstage bleeds and inlet guide vanes controlled by the average engine inlet temperature. To investigate the effects of using an engine inlet temperature different from the average, the engine was also tested with the inlet guide vane and interstage bleed schedule controlled by temperatures measured both in and out of the high temperature region. Compressor performance with the control temperature sensing thermocouples both outside and inside the high temperature region of a 180° circumferential distortion is shown in figures 18 and 19, respectively. Corrected values of speed and airflow are based on average inlet temperature and pressure. The trends of stall pressure ratio and airflow pumping capability agree with those discussed earlier for the circumferential distortion patterns. Comparison of figures 18(b) and 19(b) shows, at the lower speeds, the greatest effect on performance occurs with inlet temperature sensors located outside the high temperature region. This result was expected because the low temperatures cause the interstage bleeds to close sooner than if they were being controlled by the average or high inlet temperature.

A summary of the effect of the inlet temperature sensing location on compressor stall pressure ratio loss is presented in figure 20. With a 15 percent temperature distortion

level at corrected speeds over 90 percent there is an 8.4 percent loss of stall pressure ratio with the sensors outside the heated region compared to a value of  $\Delta$ PRS of 6.2 percent with the sensors located in the heated region. In general, the largest effect on  $\Delta$ PRS occurs when the inlet temperature sensors are outside the heated region and performance is least effected by locating the sensors in the heated region. Using average temperature (fig. 16(b)) yields  $\Delta$ PRS values that are between the aforementioned extremes.

### Combined Temperature and Pressure Distortion

Combined temperature and pressure distortions were produced by using a  $180^\circ$  circumferential extent screen in conjunction with the hydrogen burner. The screen,  $5\frac{1}{2}$  mesh by 0.137 centimeter (0.054-in.) wire diameter with a 49.6 porosity, was supported on a 1 mesh, 84.6 percent porosity grid structure located approximately one engine diameter upstream of the compressor inlet. This screen installation is the same as described in reference 1. A total pressure distortion of 7.0 percent ( $1 - (P_{t,2})_{\min} / (P_{t,2})_{\text{avg}}$ ) was generated at rated engine speed.

A typical profile of combined distortion is shown in figure 21. In this case the high temperature and low pressure regions are at the same circumferential location at the engine inlet. For all testing with the combined distortion the low pressure region was at the same location (top half of compressor face) and the high temperature region was indexed around the inlet.

The effect of combined temperature and pressure distortions on compressor performance is shown in figure 22. The greatest performance degradations resulted with the high temperature and low pressure regions at the same location (figs. 22(a) and (b)) to provide the lowest air density. The smallest effect was realized when the high temperature was opposite the low pressure (figs. 22(e) and (f)) and density variations were reduced.

The combined patterns of figures 22(d) and 22(g) were tested to determine if any rotational effects existed. It appears that some effects do exist because the engine was more sensitive, at the lower speeds, when the high temperature region was on the right side of the compressor inlet.

A summary of the effect of the relative location of the high temperature and low pressure regions on compressor stall pressure ratio is presented in figure 23. At 99 percent corrected speed, with the same distortion levels, the compressor stall pressure ratio was 7.51 with the high temperature and low pressure regions diametrically opposed whereas the stall pressure ratio was 7.10 when these regions coincided. With the opposing distortions, the data of figure 23 shows an improvement in stall pressure ratio

at the low corrected speeds. However, this does not take into account the reduction in compressor airflow caused by the distortion.

## SUMMARY OF RESULTS

A J85-GE-13 turbojet engine was subjected to steady-state temperature and combined temperature and pressure distortions to investigate their effect on compressor operating limits and performance. The temperature distortions were produced by a hydrogen burner located upstream of the compressor inlet. The combined distortions utilized a screen located about one engine diameter upstream of the compressor face to create the pressure distortion. Data were obtained for various extents and magnitudes of circumferential temperature distortion and two levels of hub radial distortion. Studies with the combined temperature and pressure distortion included varying the relative positions of the high temperature and low pressure regions at the compressor face. Correlations were made to show the effect of the distortions on compressor stall pressure ratio. The following results were obtained:

1. As a function of distortion level, the hub-radial pattern caused the largest compressor stall pressure ratio loss.
2. The loss of stall pressure ratio for the circumferential temperature distortion patterns was dependent on both extent and magnitude with the 180<sup>0</sup> extent causing the largest losses.
3. A pattern of diametrically opposed 90<sup>0</sup> sectors had a smaller effect on compressor performance than a single sector of the same magnitude. This multiple pattern caused the smallest performance degradation of all distortions tested.
4. Compressor stall pressure ratio loss as a function of distortion level was found to be dependent on corrected speed.
5. Deterioration of compressor performance and operating limits when operating with combined temperature and pressure distortion was dependent on the relative position of the high temperature and low pressure regions. The most serious effect occurred when these regions were at the same location and the smallest effect resulted with the high temperature and low pressure regions diametrically opposed.
6. The effect of circumferential temperature distortion was found to be more severe as the inlet Reynolds number index was reduced.

Lewis Research Center,  
National Aeronautics and Space Administration,  
Cleveland, Ohio, October 2, 1973,  
501-24.

## APPENDIX A

### SYMBOLS

A	area, m <sup>2</sup> (in. <sup>2</sup> )
N	engine speed, percent of rated (16 500 rpm)
P	pressure, N/m <sup>2</sup> (psia)
Δ PRS	compressor stall pressure ratio loss,

$$1 - \left[ \left( \frac{P_{t,3}}{P_{t,2}} \right)_{\text{distorted}} / \left( \frac{P_{t,3}}{P_{t,2}} \right)_{\text{undistorted}} \right]$$

ReI	Reynolds number index, $\delta / \varphi \sqrt{\theta}$
T	total temperature, K( <sup>0</sup> R)
W	flowrate, kg/sec (lb/sec)
δ	ratio of total pressure to absolute pressure of NACA standard sea-level conditions
θ	ratio of total temperature to absolute temperature of NACA standard sea-level conditions
φ	ratio of viscosity to viscosity at NACA standard sea-level conditions

#### Subscripts:

a	air
avg	average
cir	circumferential average of all probes at the same immersion depth
distorted	with inlet distortion
max	maximum
min	minimum
p	inlet air plenum
rad	radial average of all probes at the same circumferential location

t	total conditions
undistorted	without inlet distortion
2	compressor inlet
3	compressor discharge
8	exhaust nozzle exit

## APPENDIX B

### METHODS OF CALCULATION

#### Engine Airflow

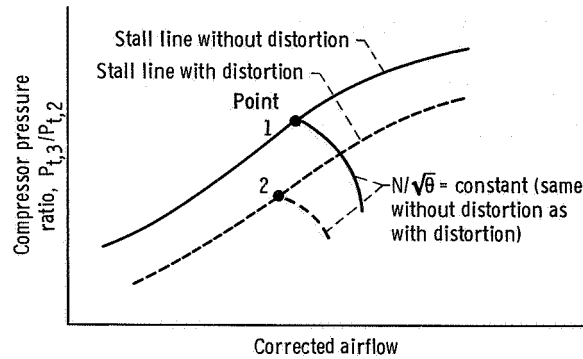
The engine airflow was determined from total pressure and temperature measurements at the inlet plenum and static pressures at station 1 using the continuity equation. The inlet air bellmouth had a previously determined flow coefficient of 0.985 repeatable to  $\pm 0.3$  percent and the engine had been run without the burner installed so its airflow characteristics were known. With the burner installed, data with uniform inlet flow were obtained and the flow coefficient was adjusted to make the two sets of data agree. This new value of flow coefficient, 0.918, was then used to calculate the effective area of the airflow measuring station. The corrected engine airflow was then calculated based on the average total pressure and temperature at the compressor inlet (station 2).

#### Stall Conditions

The values of compressor pressure ratio and corrected airflow at stall were obtained by extrapolation. Stall points were obtained by slowly closing the exhaust nozzle area at a constant corrected speed and observing the turbine discharge temperature at stall. Steady-state data points were also taken along the constant speed line. The steady-state point closest to stall was usually within 28 K (50 F) of the turbine discharge temperature at stall. Curves were then drawn of compressor pressure ratio and corrected airflow as a function of turbine discharge temperature and extrapolated to the stall temperature to determine the engine operating point at stall.

## Compressor Stall Pressure Ratio Loss

The loss of compressor stall pressure ratio when operating with distortion was calculated using the same corrected speed to determine the stall pressure ratios for the distorted and undistorted cases. The method is illustrated in the following sketch:



The compressor stall pressure ratio loss  $\Delta \text{PRS}$  is then defined as the difference in pressure ratio between points 1 and 2 divided by the pressure ratio at point 1 or

$$\Delta \text{PRS} = 1 - \left[ \left( \frac{P_{t,3}}{P_{t,2}} \right)_{\text{distorted}} / \left( \frac{P_{t,3}}{P_{t,2}} \right)_{\text{undistorted}} \right]$$

## REFERENCES

1. Calogeras, James E.; Mehalic, Charles M.; and Burstadt, Paul L.: Experimental Investigation of the Effect of Screen-Induced Total-Pressure Distortion on Turbojet Stall Margin. NASA TM X-2239, 1971.
2. McAulay, John E.: Effect of Dynamic Variations in Engine - Inlet Pressure on the Compressor System of a Twin-Spool Turbofan Engine. NASA TM X-2081, 1970.
3. Werner, Roger A.; Abdelwahab, Mahmood; and Braithwaite, Willis M.: Performance and Stall Limits of an Afterburner-Equipped Turbofan Engine with and Without Inlet Flow Distortion. NASA TM X-1947, 1970.
4. Rudey, Richard A.; and Antl, Robert J.: The Effect of Inlet Temperature Distortion on the Performance of a Turbo-Fan Engine Compressor System. NASA TM X-52788, 1970.
5. Braithwaite, Willis M.: Experimental Evaluation of a TF 30-P-3 Turbofan Engine in an Altitude Facility: Effect of Steady-State Temperature Distortion. NASA TM X-2921, 1973.
6. Glawe, George E.; Simmons, Frederick S.; and Stickney, Truman M.: Radiation and Recovery Corrections and Time Constants of Several Chromel-Alumel Thermocouple Probes in High-Temperature, High-Velocity Gas Streams. NACA TN 3766, 1956.
7. Staff of Lewis Laboratory: Central Automatic Data Processing System. NACA TN 4212, 1958.

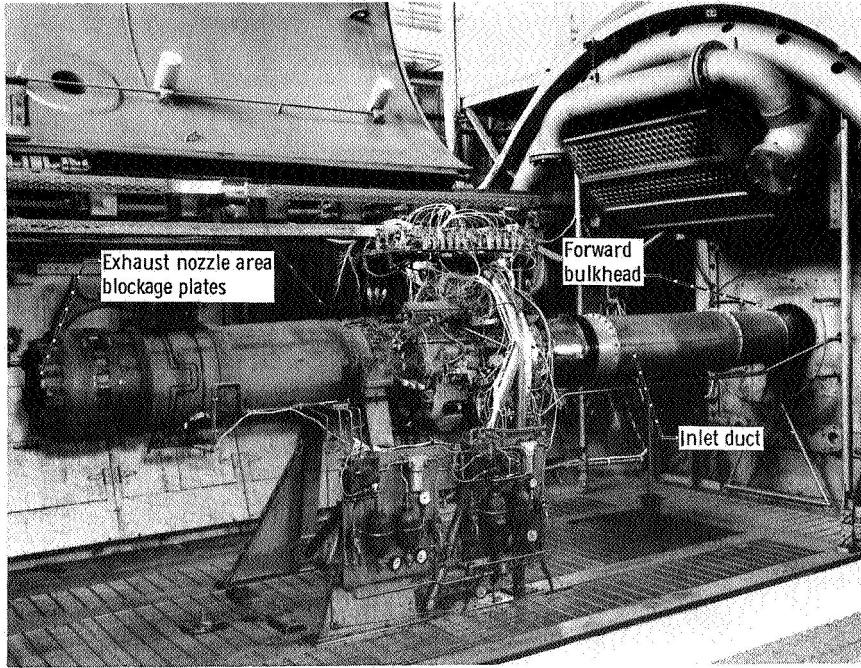


Figure 1. - J85-GE-13 installed in altitude chamber.

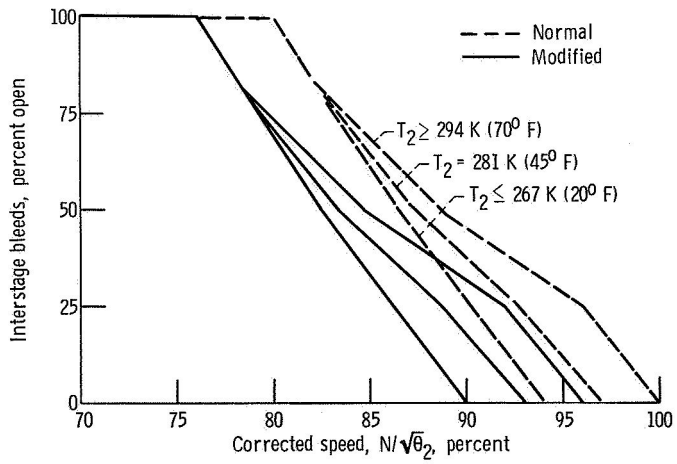
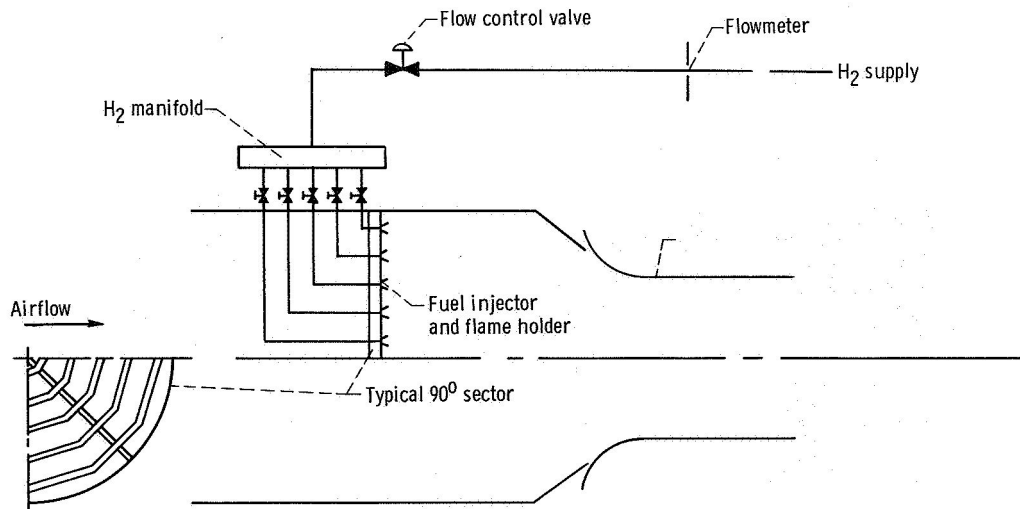
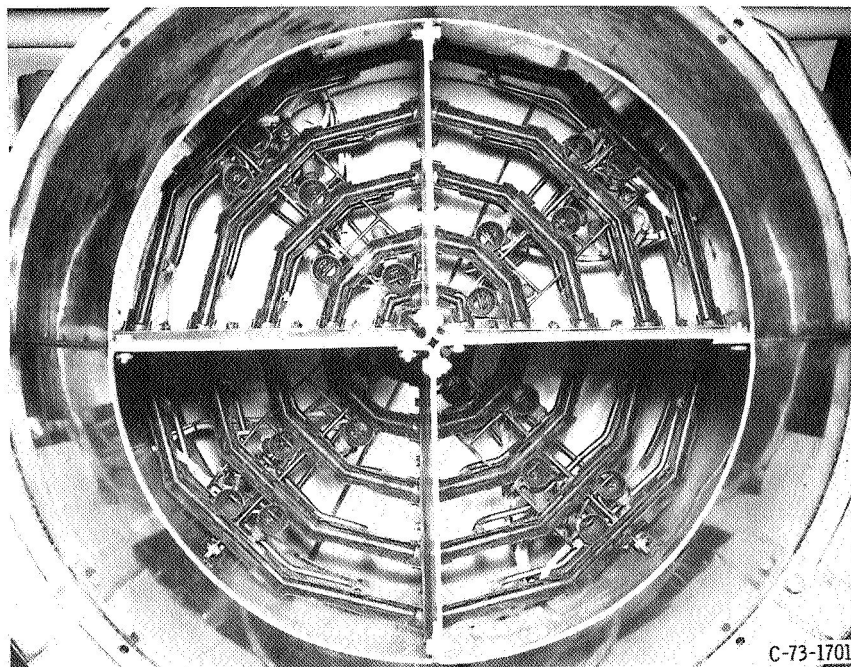


Figure 2. - J85-GE-13 compressor interstage bleed schedule where  $T_2$  is compressor inlet total temperature.



(a) Schematic of installation.



(b) Photograph looking upstream.

Figure 3. - Hydrogen fueled temperature distortion generator.

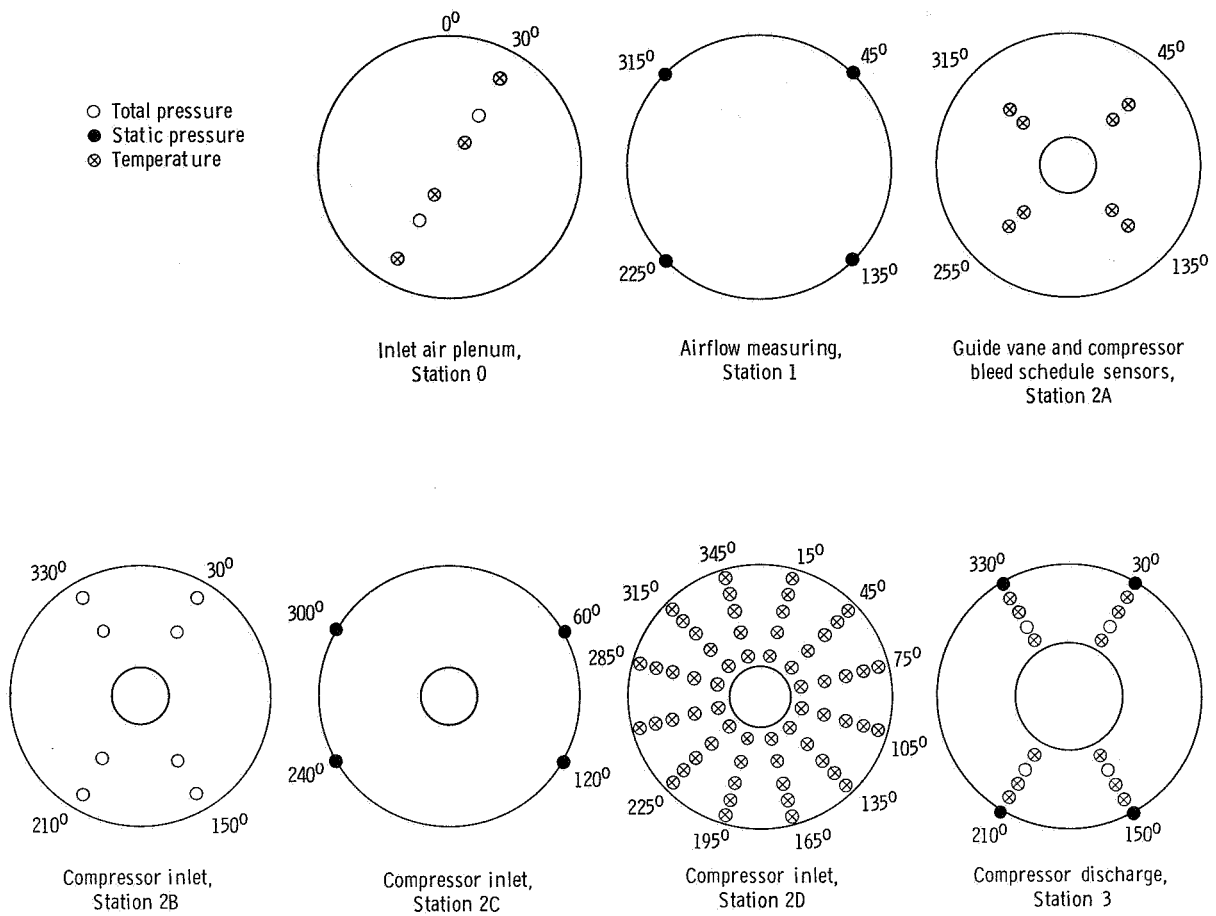
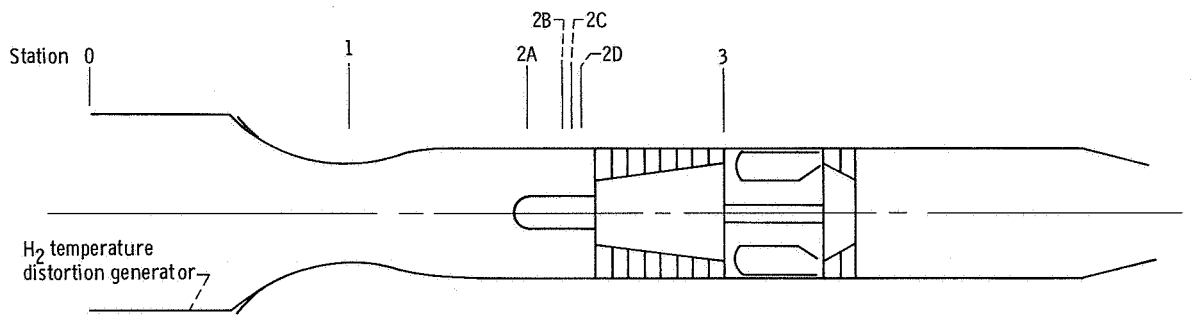


Figure 4. - Schematic of J-85-GE-13 engine measuring stations and instrumentation (all views looking upstream).

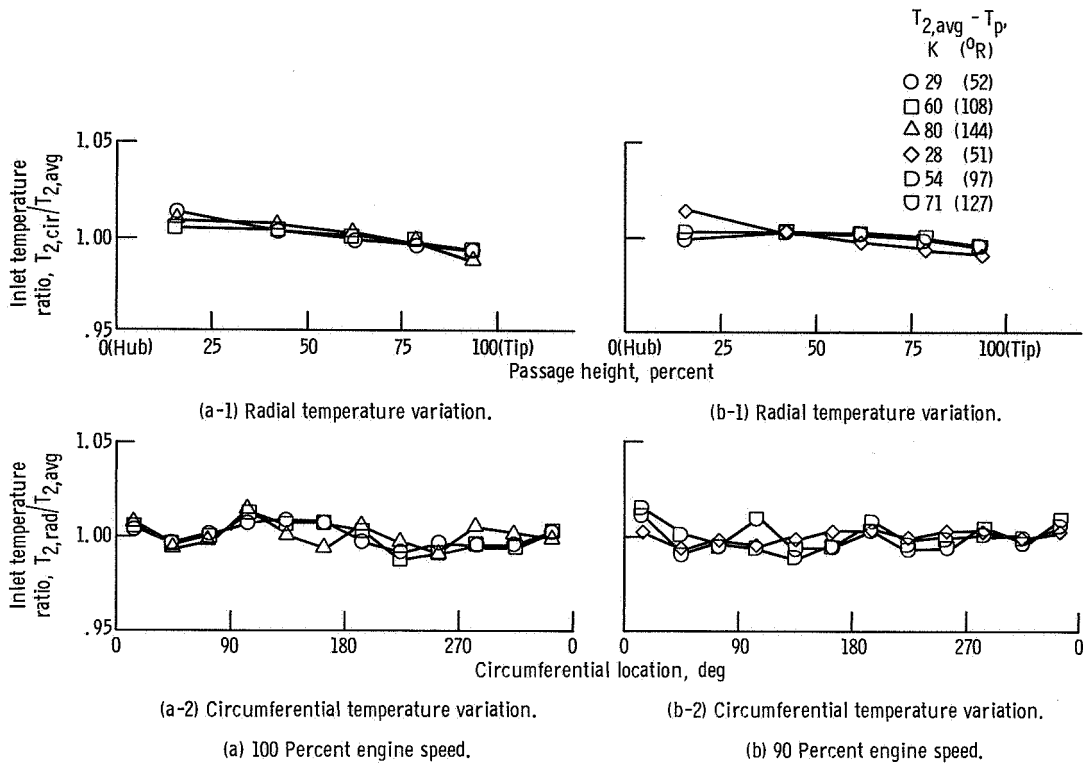


Figure 5. - Engine inlet temperature profiles with full-face burning.

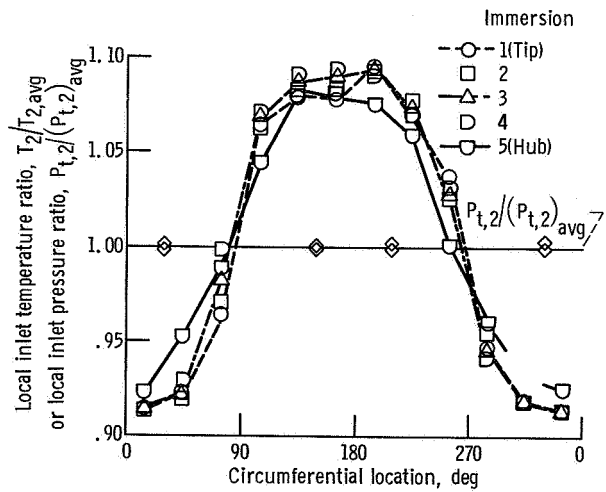


Figure 6. - Typical inlet temperature distortion pattern of 180° circumferential extent.

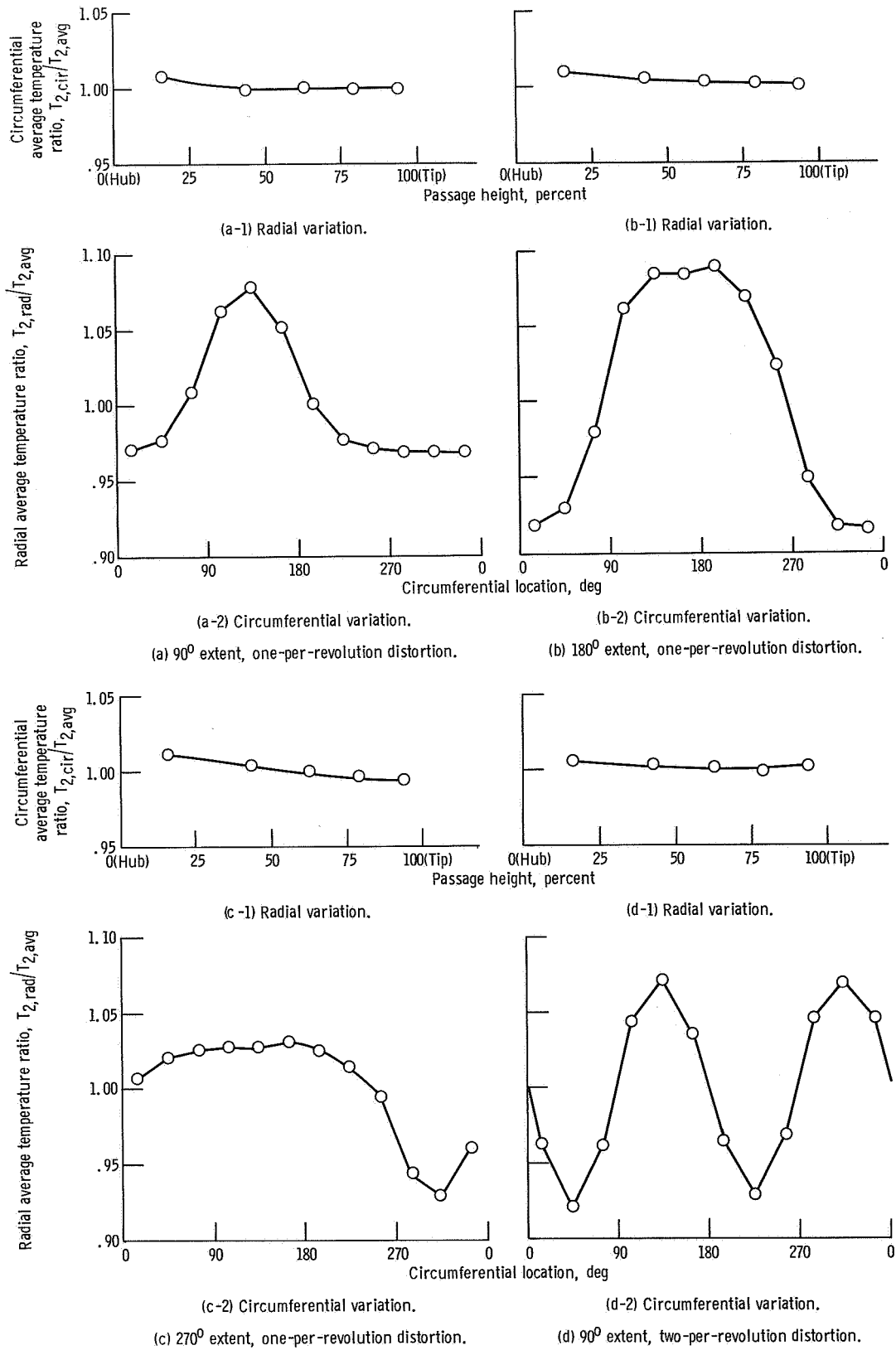
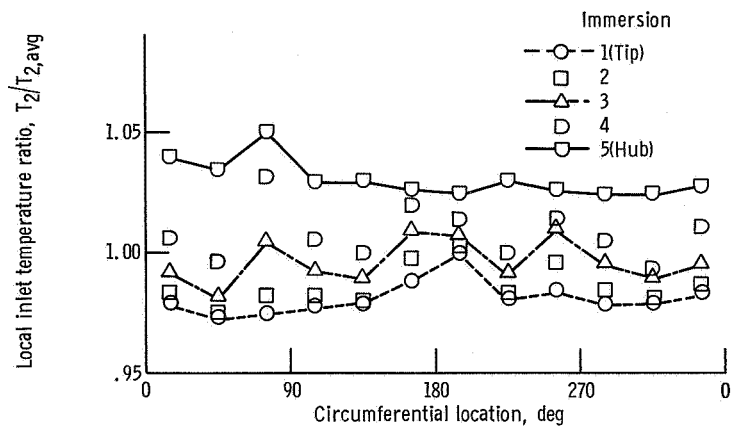


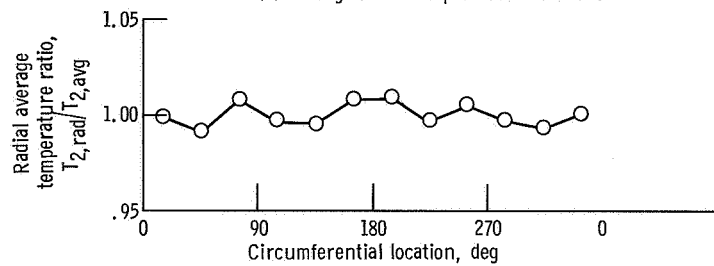
Figure 7. - Radial and circumferential temperature variations for circumferential distortion patterns.



(a) Local inlet temperature distribution.

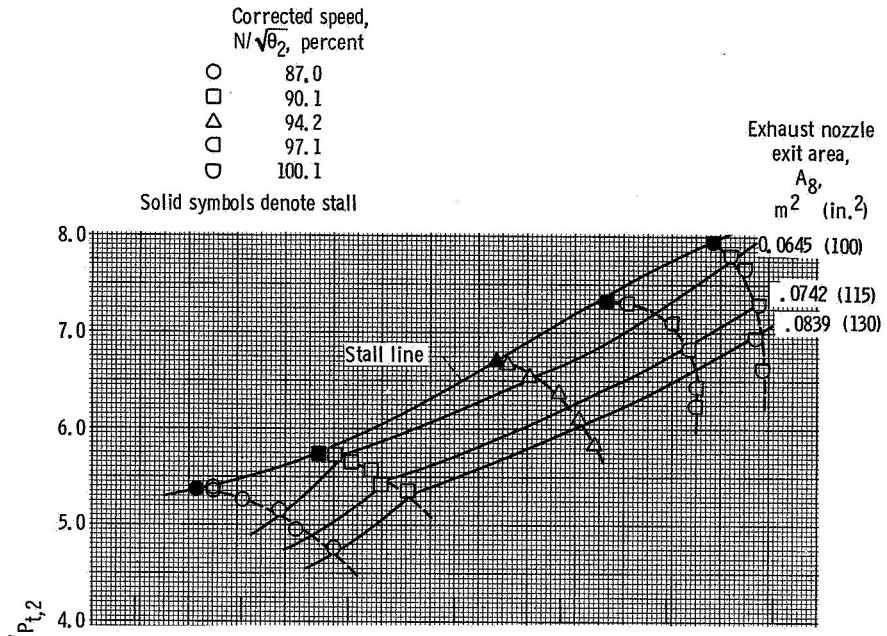


(b) Average radial temperature variation.

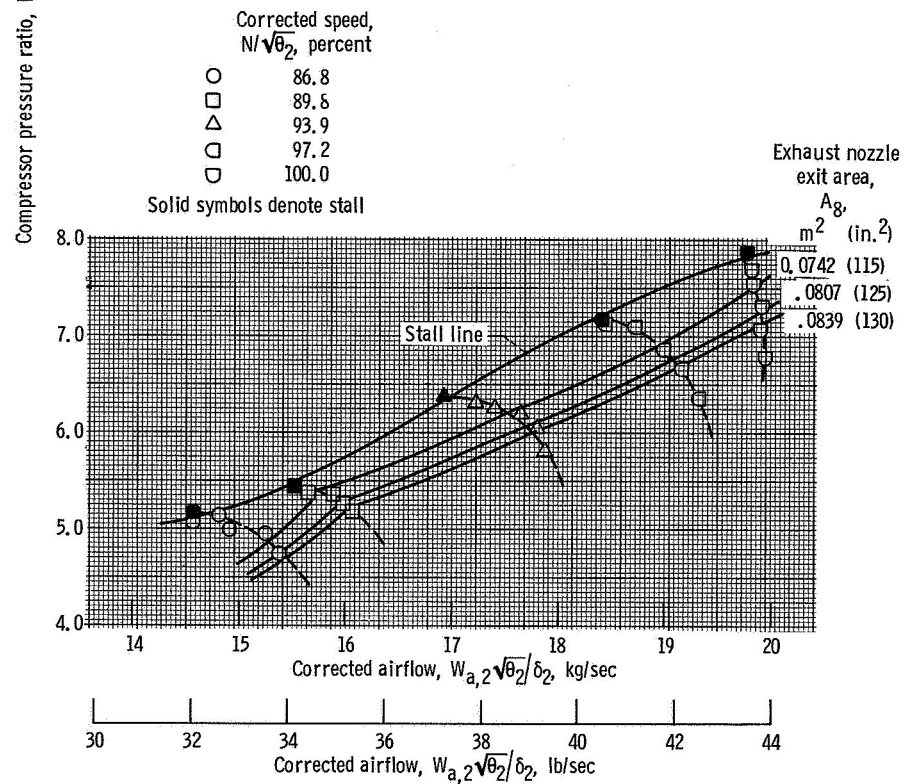


(c) Average circumferential temperature variation.

Figure 8. - Compressor inlet temperature profiles with hub radial distortion.



(a) Engine-inlet Reynolds number index  $ReI_2 = 0.65$ .



(b) Engine-inlet Reynolds number index  $ReI_2 = 0.30$ .

Figure 9. - Compressor maps with uniform inlet flow.

$\frac{T_{2,max} - T_{2,min}}{T_{2,avg}}$	Corrected speed, $N/\sqrt{\theta_2}$ , percent
○ - 0.050	100.1
□ .057	94.4
△ .066	86.4
◇ .119	99.2
◇ .102	93.3
◇ .136	85.7
◇ .212	97.8
◇ .197	91.9
◇ .191	85.4



Solid symbols denote stall  
Constant speed lines are for same  $N/\sqrt{\theta_2}$   
for distorted and undistorted flow

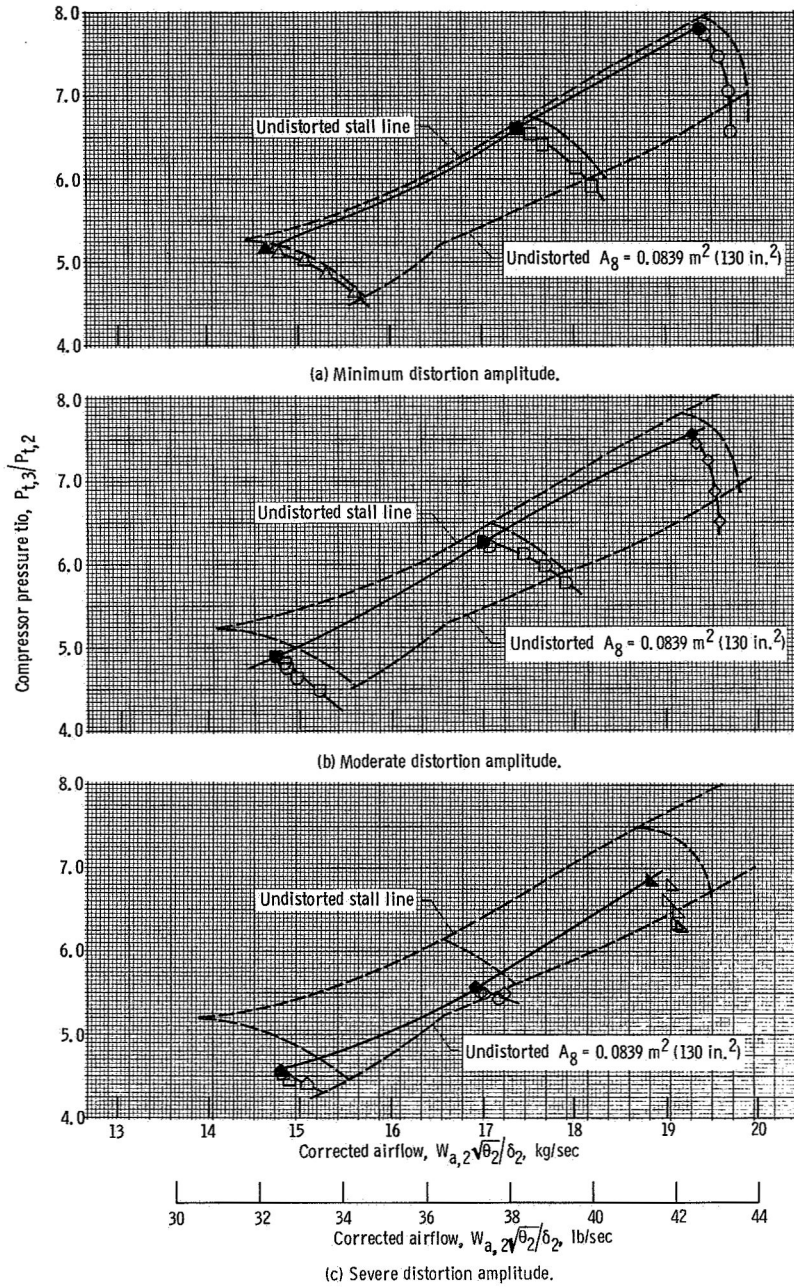


Figure 10. - Compressor performance with 90° extent circumferential distortion. Engine-inlet Reynolds number index  $Re_{I_2} = 0.65$ .

	$T_{2,max} - T_{2,min}$	Corrected speed,
	$T_{2,avg}$	$N/\sqrt{\theta_2}$ , percent
○	0.064	99.6
□	.072	93.4
△	.081	86.0
◇	.154	94.2
◊	.146	92.3
◑	.164	85.5
◒	.181	96.2
◓	.195	93.1
◔	.184	86.9



Solid symbols denote stall  
Constant speed lines are for same  $N/\sqrt{\theta_2}$   
for distorted and undistorted flow

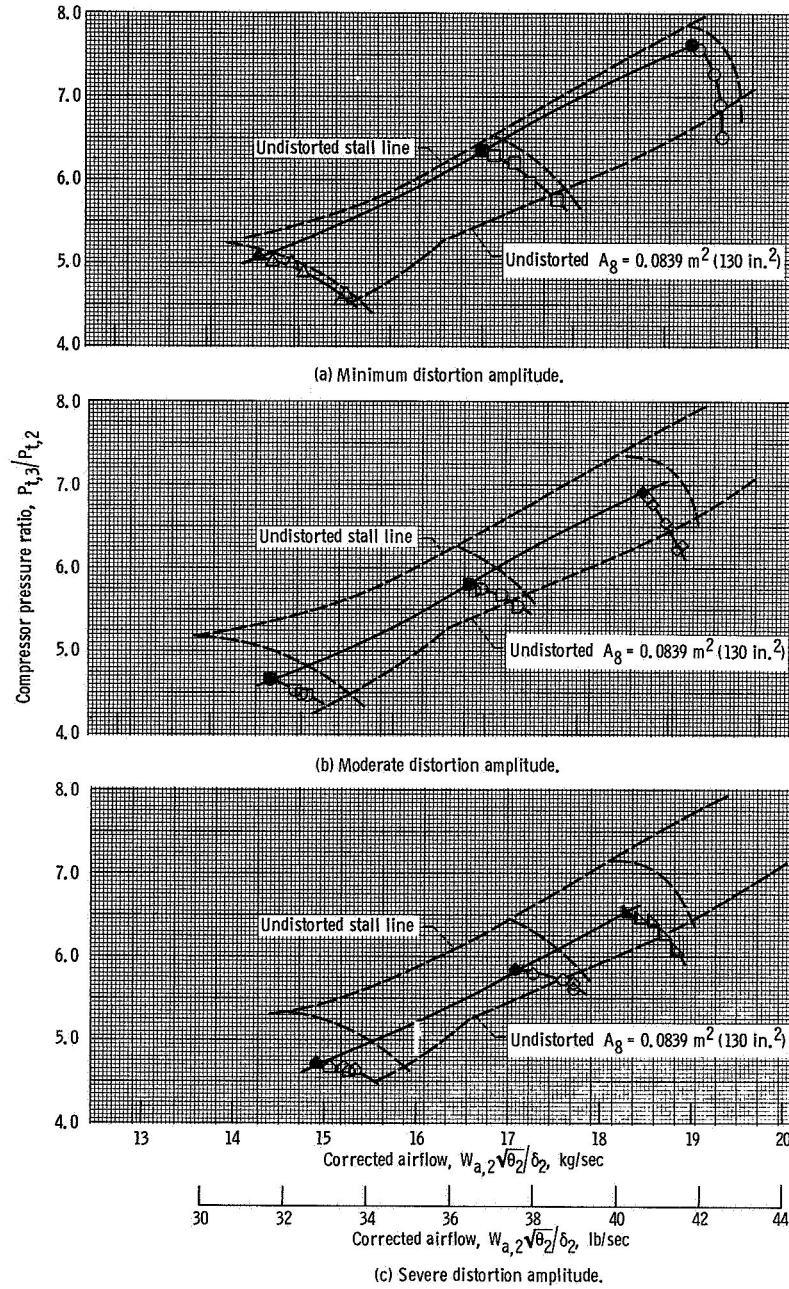
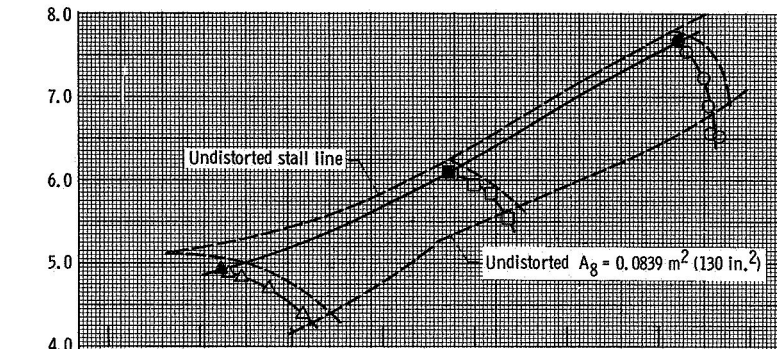


Figure 11. - Compressor performance with 180° extent circumferential distortion. Engine-inlet Reynolds number index  $Re_{I_2} = 0.65$ .

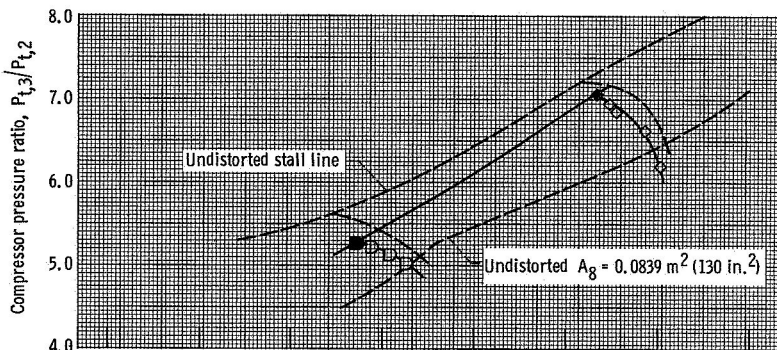
	$\frac{T_{2,max} - T_{2,min}}{T_{2,avg}}$	Corrected speed, $N/\sqrt{\theta_2}$ , percent
○	0.074	99.2
□	.087	92.3
△	.096	85.0
◇	.12	96.5
◇	.15	89.2
◇	.191	93.0
△	.181	88.3
◇	.194	84.5



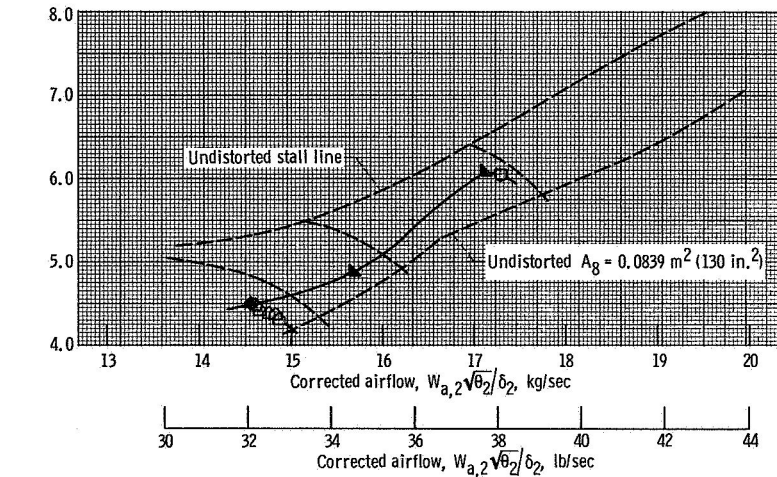
Solid symbols denote stall  
Constant speed lines are for same  $N/\sqrt{\theta_2}$   
for distorted and undistorted flow



(a) Minimum distortion amplitude.



(b) Moderate distortion amplitude.



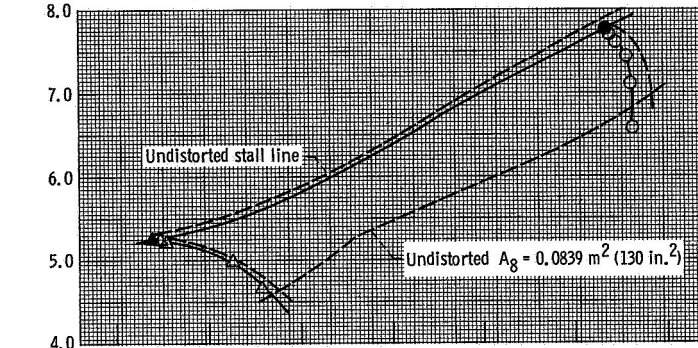
(c) Severe distortion amplitude.

Figure 12. - Compressor performance with 270° extent circumferential distortion. Engine-inlet Reynolds number index  $Re_{I_2} = 0.65$ .

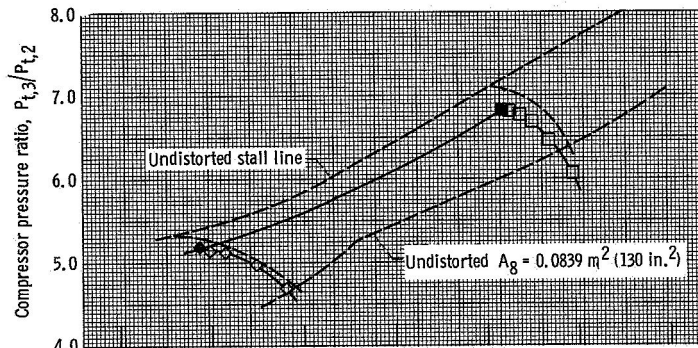
$\frac{T_{2,max} - T_{2,min}}{T_{2,avg}}$	Corrected speed, $N/\sqrt{\theta_2}$ , percent
○ 0.045	99.6
△ .066	86.5
□ .164	95.9
◇ .172	87.0
◇ .183	95.0
□ .187	86.0



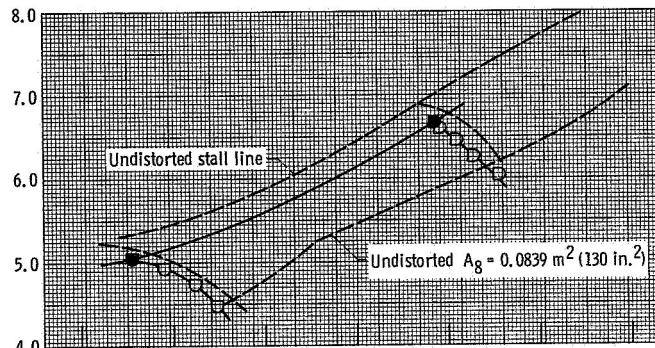
Solid symbols denote stall  
Constant speed lines are for same  $N/\sqrt{\theta_2}$   
for distorted and undistorted flow



(a) Minimum distortion amplitude.



(b) Intermediate distortion amplitude.



(c) Strong distortion amplitude.

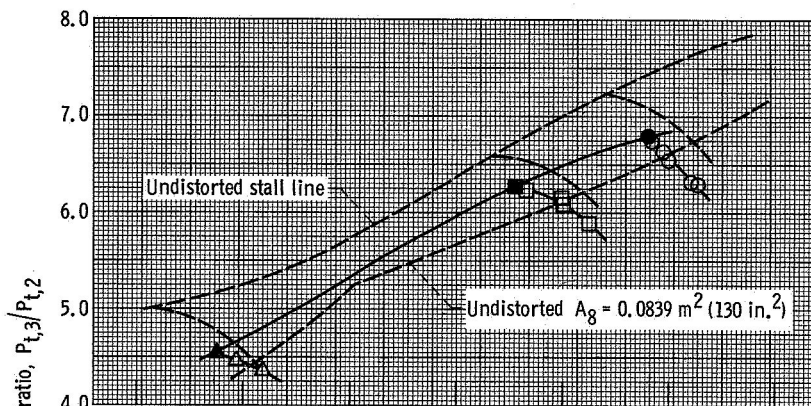
Corrected airflow,  $W_{a,2}\sqrt{\theta_2}/\delta_2$ , lb/sec  
30 32 34 36 38 40 42 44

Figure 13. - Compressor performance with  $90^\circ$  extent, two-per-revolution distortion. Engine-inlet Reynolds number index  $ReI_2 = 0.65$ .

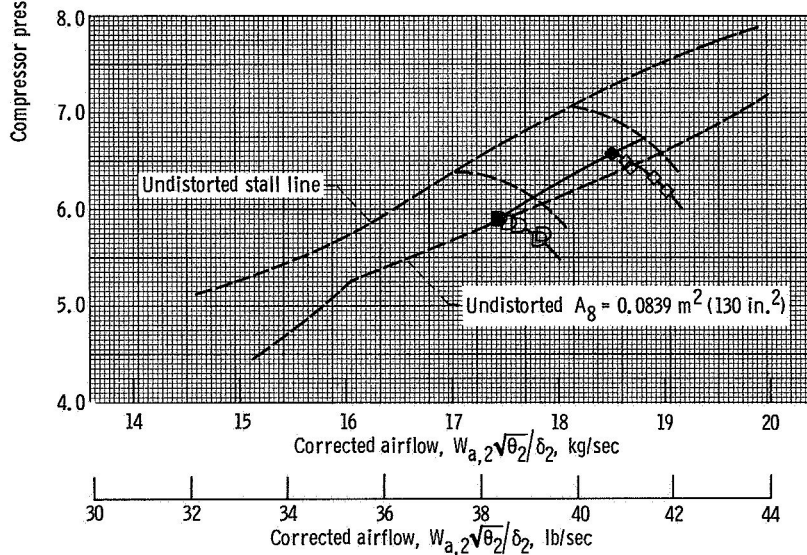
	$\frac{T_{2,max} - T_{2,min}}{T_{2,avg}}$	Corrected speed, $N/\sqrt{\theta_2}$ percent
○	0.133	97.4
□	.119	94.8
△	.134	85.3
◇	.158	96.7
◇	.153	94.0



Solid symbols denote stall  
Constant speed lines are for same  $N/\sqrt{\theta_2}$   
for distorted and undistorted flow



(a) Moderate distortion amplitude.



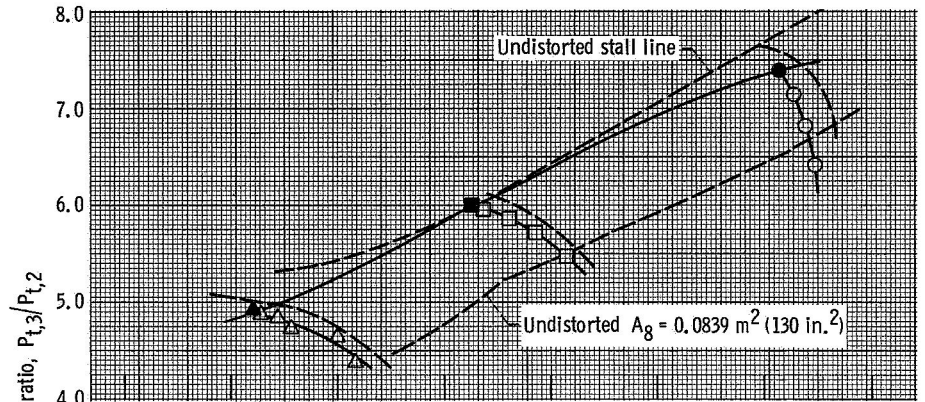
(b) Severe distortion amplitude.

Figure 14. - Compressor performance with 180° extent circumferential distortion.  
Engine-inlet Reynolds number index  $ReI_2 = 0.30$ .

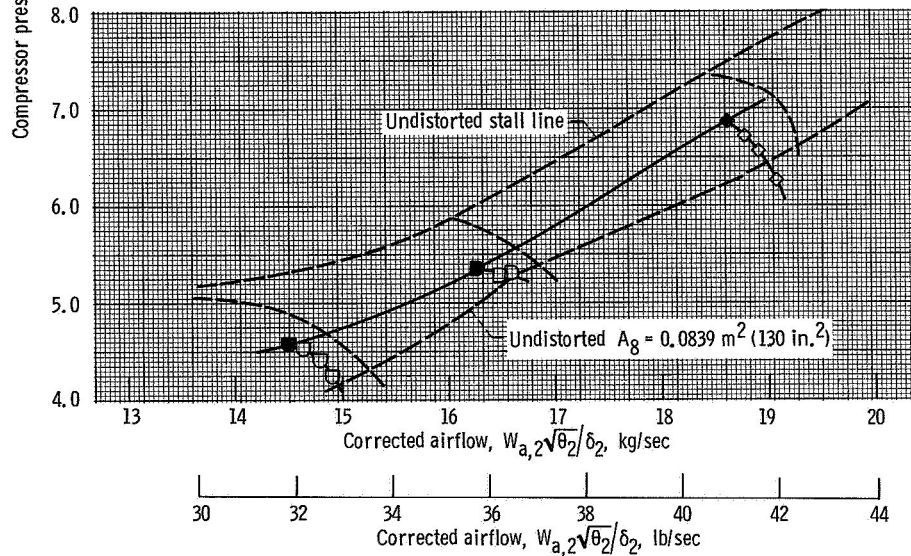
$\frac{T_{2,max} - T_{2,min}}{T_{2,avg}}$	Corrected speed, $N/\sqrt{\theta_2}$ , percent
○ 0.065	98.5
□ .078	91.7
△ .079	85.0
◇ .128	97.1
◇ .143	90.7
□ .145	84.4



Solid symbols denote stall  
 Constant speed lines are for same  $N/\sqrt{\theta_2}$   
 for distorted and undistorted flow



(a) Minimum distortion amplitude.



(b) Moderate distortion amplitude.

Figure 15. - Compressor performance with hub radial distortion. Engine-inlet Reynolds number index  $Re_{I_2} = 0.65$ .

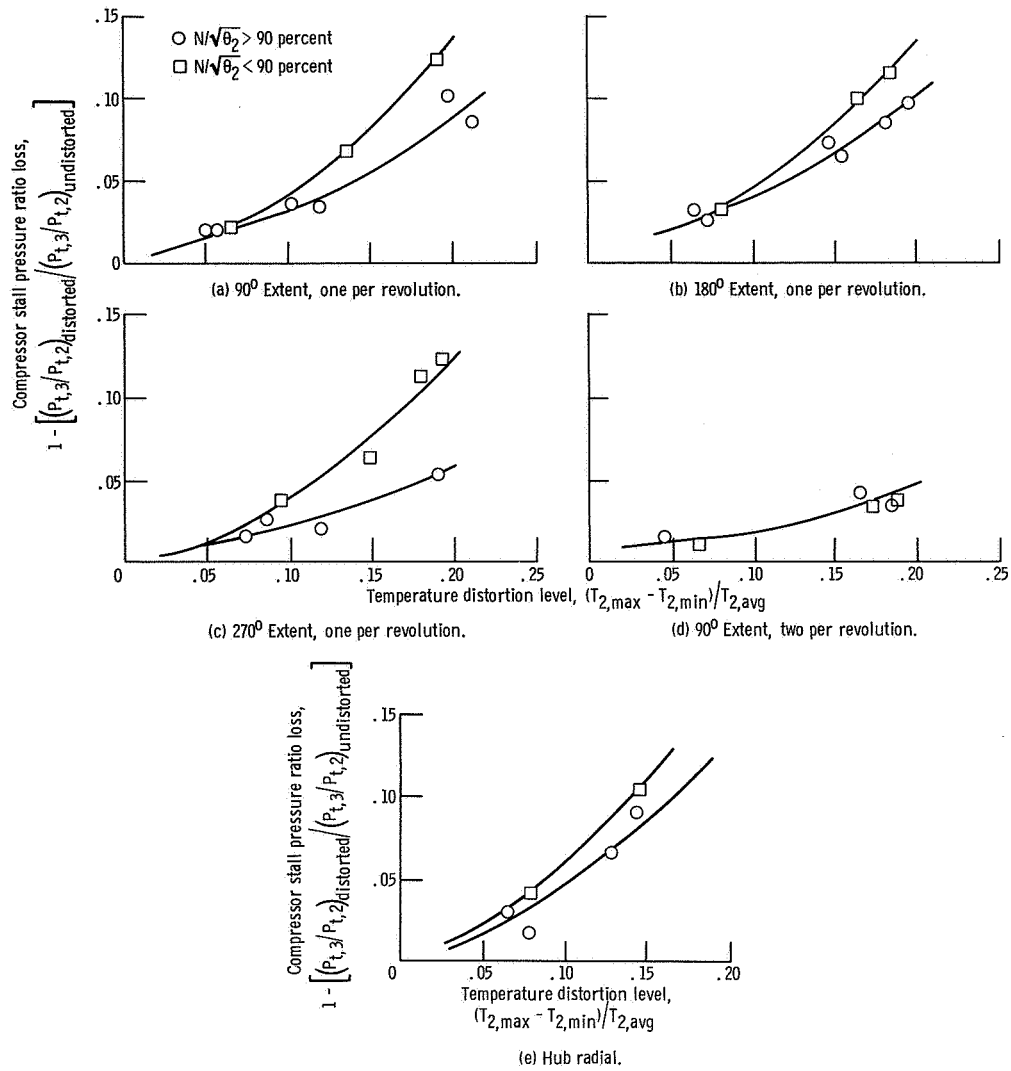


Figure 16. - Effect of inlet temperature distortion on stall pressure ratio of J-85-13 compressor.

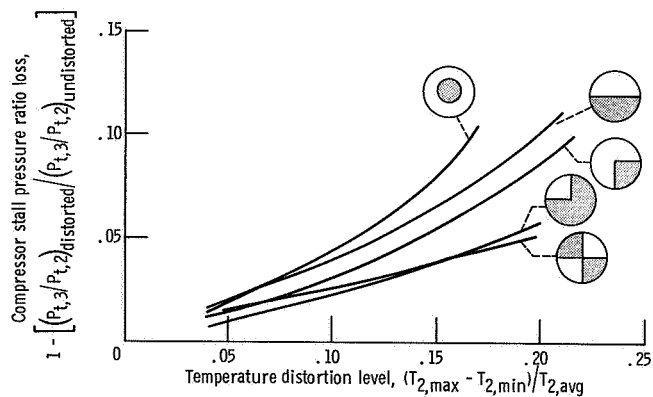
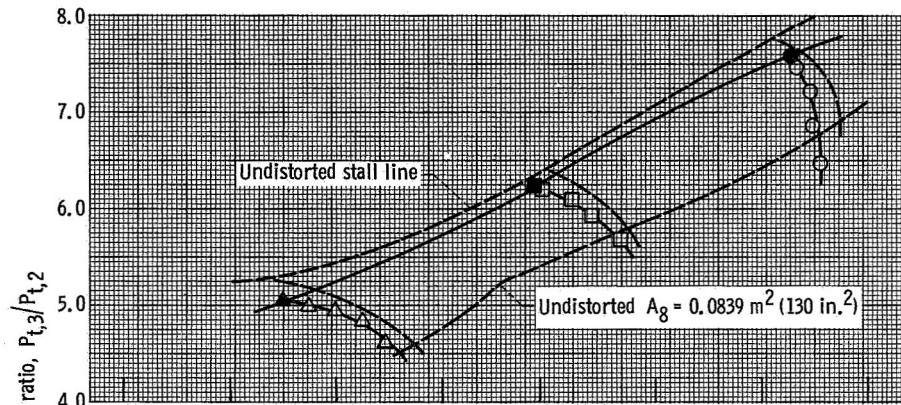


Figure 17. - Summary of temperature distortion effect on compressor stall pressure ratio loss  $N/\sqrt{B_2} > 90$  percent; Reynolds number index  $Re_I = 0.65$ . (Shaded area indicates distorted region.)

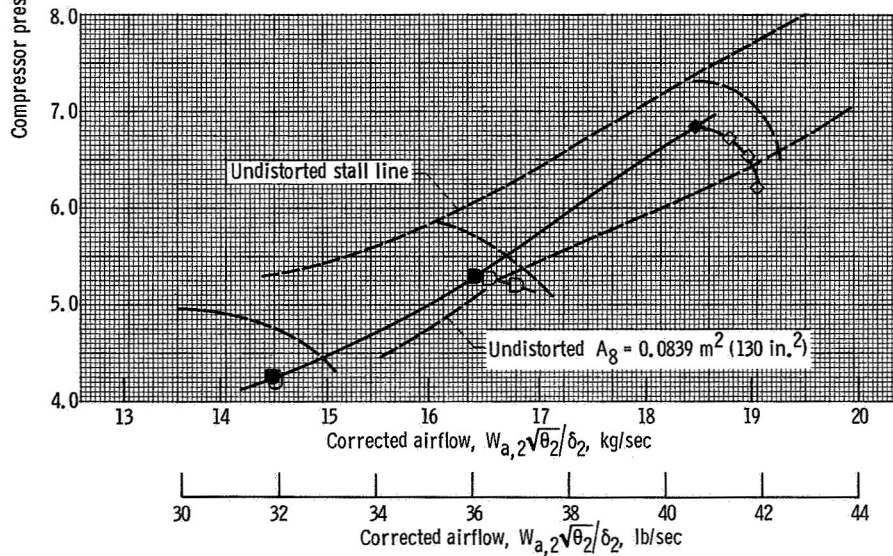
$\frac{T_{2,max} - T_{2,min}}{T_{2,avg}}$	Corrected speed, $N/\sqrt{\theta_2}$ percent
○ 0.055	99.1
□ .070	93.0
△ .076	86.4
◇ .136	97.0
◇ .162	90.7
□ .184	83.9



Solid symbols denote stall  
Constant speed lines are for same  $N/\sqrt{\theta_2}$   
for distorted and undistorted flow



(a) Minimum distortion amplitude.



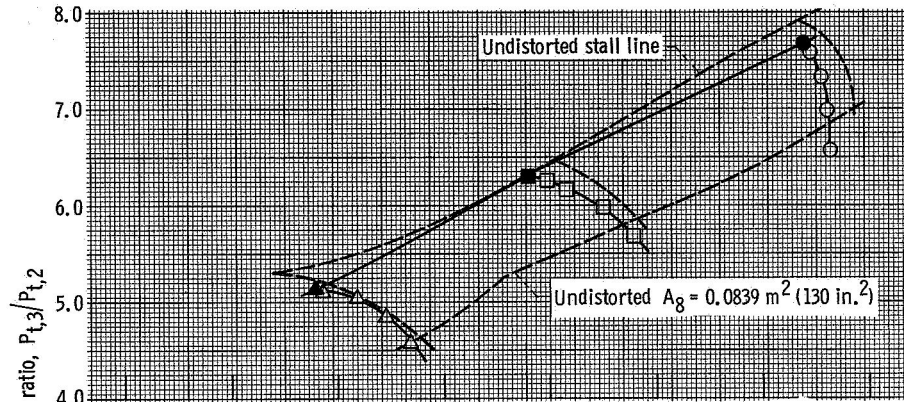
(b) Severe distortion amplitude.

Figure 18. - Compressor performance with guide-vane and bleed control temperature sensors located in unheated quadrants. Engine-inlet Reynolds number index  $Re_{I_2} = 0.65$ .

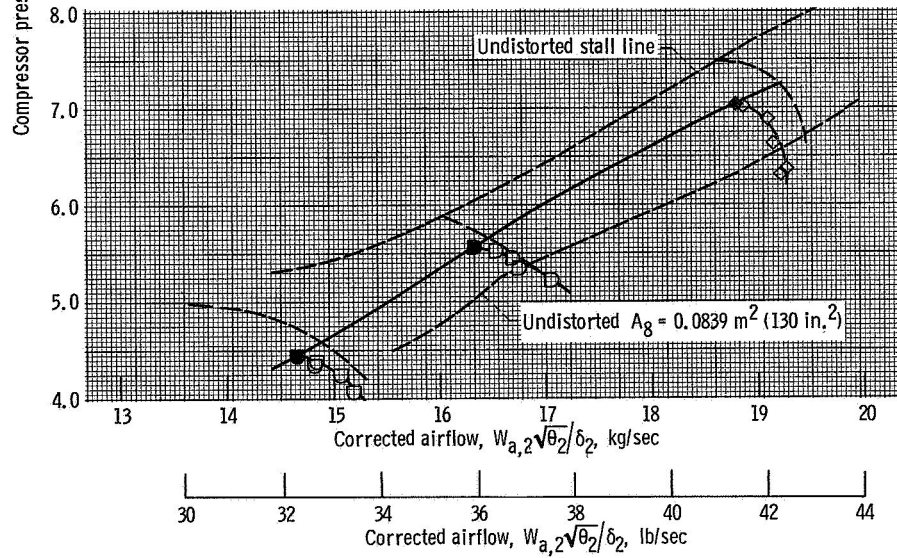
$\frac{T_{2,max} - T_{2,min}}{T_{2,avg}}$	Corrected speed, $N/\sqrt{\theta_2}$ , percent
○ 0.056	99.8
□ .065	93.2
△ .074	86.5
◇ .127	97.7
◇ .165	90.7
○ .178	84.2



Solid symbols denote stall  
Constant speed lines are for same  $N/\sqrt{\theta_2}$   
for distorted and undistorted flow



(a) Minimum distortion amplitude.



(b) Severe distortion amplitude.

Figure 19. - Compressor performance with guide-vane and bleed control temperature sensors located in heated quadrants. Engine-inlet Reynolds number index  $ReI_2 = 0.65$ .

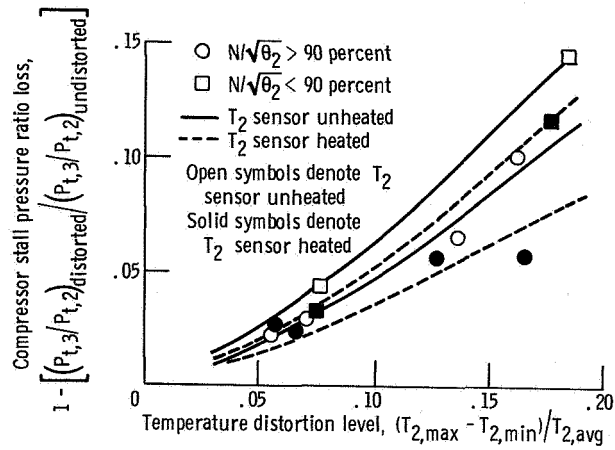


Figure 20. - Effect of inlet guide vane-interstage bleed  $T_2$  sensor location on compressor pressure ratio loss for circumferential  $180^\circ$  extent temperature distortion.

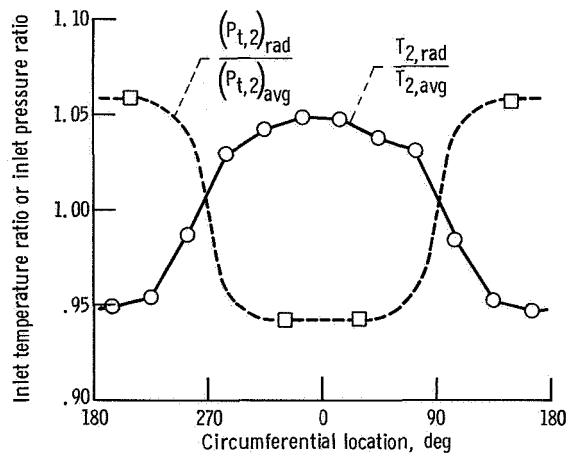
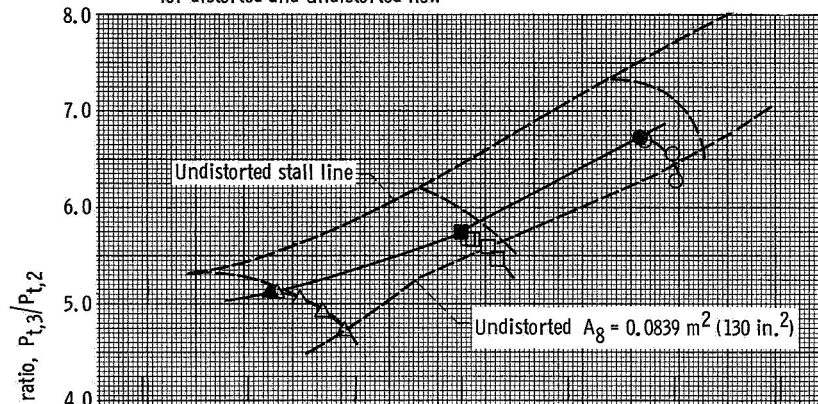


Figure 21. - Typical profiles with combined inlet distortion pattern.

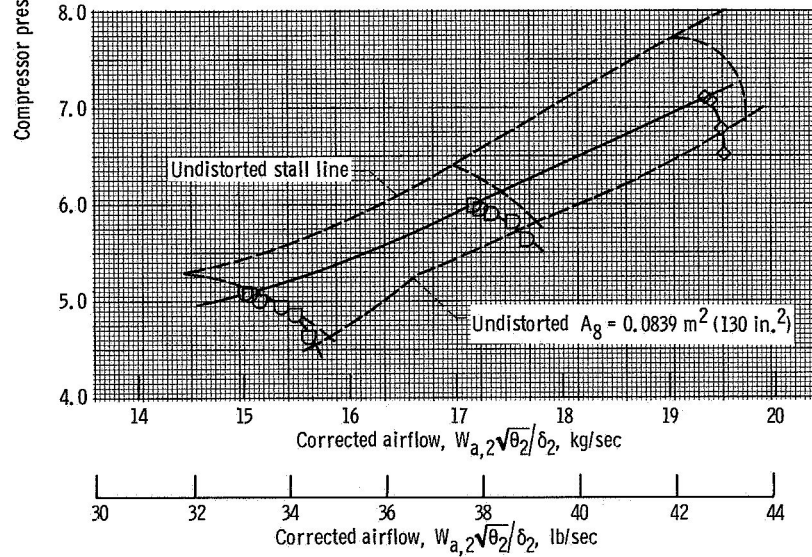
	$\frac{(P_{t,2})_{avg} - (P_{t,2})_{min}}{(P_{t,2})_{avg}}$	$\frac{T_{2,max} - T_{2,min}}{T_{2,avg}}$	Corrected speed, $N/\sqrt{\theta_2}$ , percent
○	0.07	0.067	99.0
□	.05	.067	93.0
△	.036	.074	86.6
◇	.063	.108	97.1
◻	.049	.111	92.1
◻	.036	.104	87.2



Solid symbols denote stall  
Constant speed lines are for same  $N/\sqrt{\theta_2}$   
for distorted and undistorted flow



(a) Distortions together; low temperature distortion level.



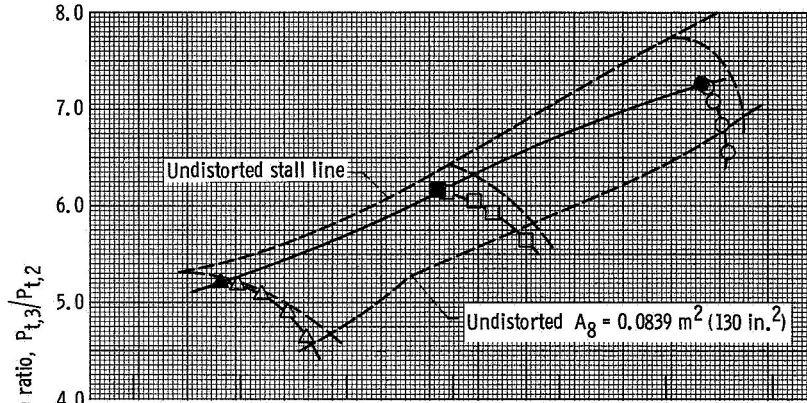
(b) Distortions together; moderate temperature distortion level.

Figure 22. - Compressor performance with combined temperature and pressure distortion. Engine-inlet Reynolds number index  $ReI_2 = 0.65$ .

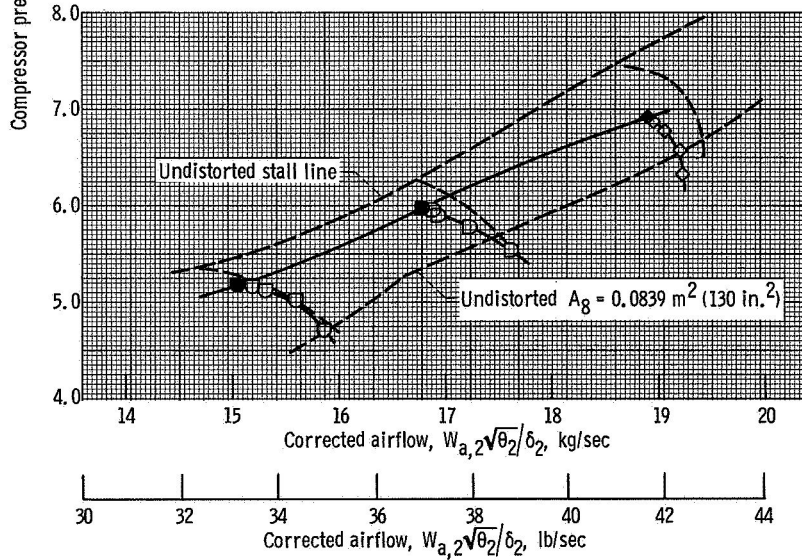
	$\frac{(P_{t,2})_{avg} - (P_{t,2})_{min}}{(P_{t,2})_{avg}}$	$\frac{T_{2,max} - T_{2,min}}{T_{2,avg}}$	Corrected speed, $N/\sqrt{\theta_2}$ , percent
○	0.07	0.065	99.0
□	.049	.063	93.0
△	.036	.073	86.8
◇	.065	.107	97.6
◊	.047	.109	92.4
◻	.036	.108	87.2



Solid symbols denote stall  
 Constant speed lines are for same  $N/\sqrt{\theta_2}$   
 for distorted and undistorted flow



(c) Distortions overlapping; low temperature distortion level.



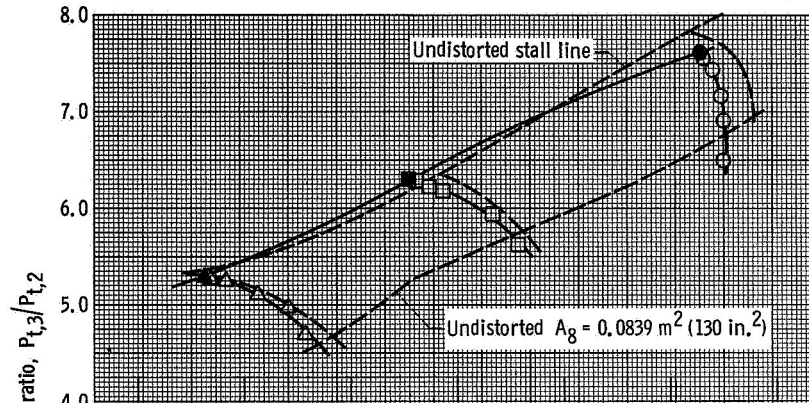
(d) Distortions overlapping; moderate temperature distortion level.

Figure 22. - Continued.

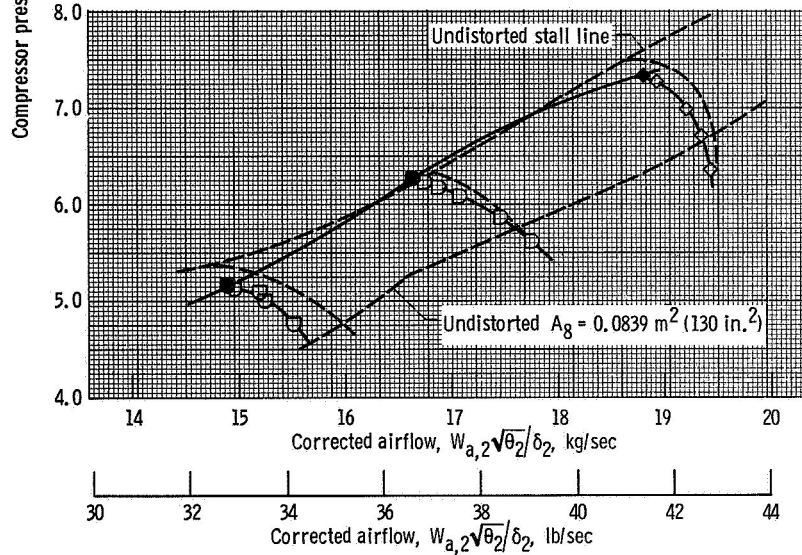
	$\frac{(P_{t,2})_{avg} - (P_{t,2})_{min}}{(P_{t,2})_{avg}}$	$\frac{T_{2,max} - T_{2,min}}{T_{2,avg}}$	Corrected speed, $N/\sqrt{\theta_2}$ percent
○	0.07	0.059	99.4
□	.046	.076	92.7
△	.033	.076	86.8
◇	.065	.112	97.8
◻	.048	.110	92.7
◻	.035	.106	87.4



Solid symbols denote stall  
 Constant speed lines are for same  $N/\sqrt{\theta_2}$   
 for distorted and undistorted flow



(e) Distortions opposed; low temperature distortion level.

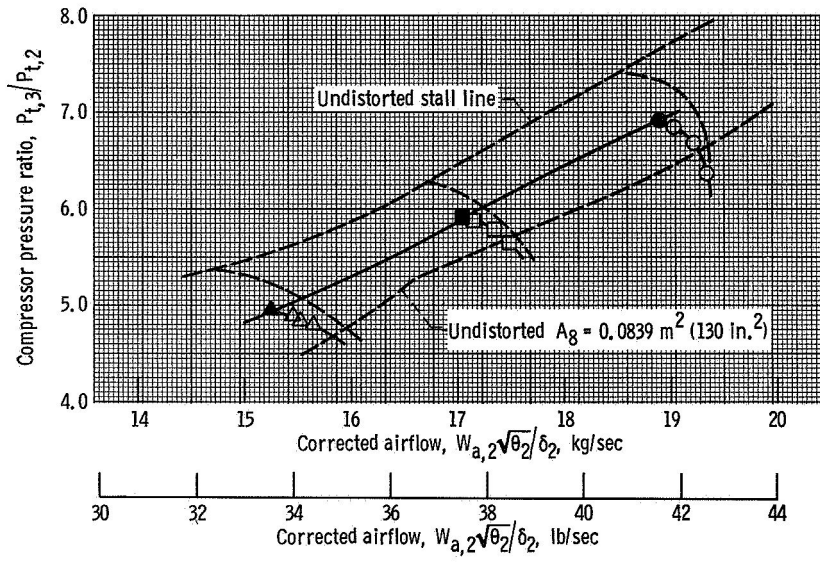


(f) Distortions opposed; moderate temperature distortion level.

Figure 22. - Continued.

	$\frac{(P_{t,2})_{avg} - (P_{t,2})_{min}}{(P_{t,2})_{avg}}$	$\frac{T_{2,max} - T_{2,min}}{T_{2,avg}}$	Corrected speed, $N/\sqrt{\theta_2}$ , percent
○	0.065	0.104	97.4
□	.050	.117	92.5
△	.038	.101	87.3

Solid symbols denote stall  
Constant speed lines are for same  $N/\sqrt{\theta_2}$   
for distorted and undistorted flow



(g) Distortions overlapping; moderate temperature distortion level.  
Figure 22. - Concluded.

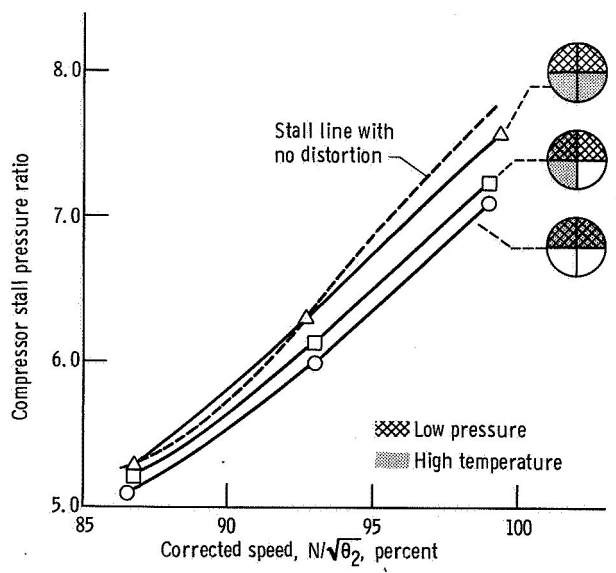


Figure 23. - Effect of relative location of high temperature and low pressure regions on turbojet stall pressure ratio with combined distortion.  $5\frac{1}{2}$  Mesh by 0.054-wire-diameter screen;  $(T_{2,max} - T_{2,min})/T_{2,avg} \sim 0.07$ .



POSTMASTER: If Undeliverable (Section 158  
Postal Manual) Do Not Return

*"The aeronautical and space activities of the United States shall be conducted so as to contribute . . . to the expansion of human knowledge of phenomena in the atmosphere and space. The Administration shall provide for the widest practicable and appropriate dissemination of information concerning its activities and the results thereof."*

—NATIONAL AERONAUTICS AND SPACE ACT OF 1958

## NASA SCIENTIFIC AND TECHNICAL PUBLICATIONS

**TECHNICAL REPORTS:** Scientific and technical information considered important, complete, and a lasting contribution to existing knowledge.

**TECHNICAL NOTES:** Information less broad in scope but nevertheless of importance as a contribution to existing knowledge.

**TECHNICAL MEMORANDUMS:** Information receiving limited distribution because of preliminary data, security classification, or other reasons. Also includes conference proceedings with either limited or unlimited distribution.

**CONTRACTOR REPORTS:** Scientific and technical information generated under a NASA contract or grant and considered an important contribution to existing knowledge.

**TECHNICAL TRANSLATIONS:** Information published in a foreign language considered to merit NASA distribution in English.

**SPECIAL PUBLICATIONS:** Information derived from or of value to NASA activities. Publications include final reports of major projects, monographs, data compilations, handbooks, sourcebooks, and special bibliographies.

**TECHNOLOGY UTILIZATION PUBLICATIONS:** Information on technology used by NASA that may be of particular interest in commercial and other non-aerospace applications. Publications include Tech Briefs, Technology Utilization Reports and Technology Surveys.

*Details on the availability of these publications may be obtained from:*

**SCIENTIFIC AND TECHNICAL INFORMATION OFFICE**

**NATIONAL AERONAUTICS AND SPACE ADMINISTRATION**

**Washington, D.C. 20546**